

Irrigant flow in the root canal: experimental validation of an unsteady Computational Fluid Dynamics model using high-speed imaging

C. Boutsoukis^{1,2}, B. Verhaagen³, M. Versluis³, E. Kastrinakis⁴ & L. W. M. van der Sluis²

¹Department of Endodontology, Dental School, Aristotle University of Thessaloniki, Thessaloniki, Greece; ²Department of Cariology, Endodontology, Pedodontlogy, Academic Centre for Dentistry Amsterdam (ACTA), Amsterdam, The Netherlands; ³Physics of Fluids Group, Faculty of Science and Technology and Research Institute for Biomedical Technology and Technical Medicine MIRA, University of Twente, Enschede, The Netherlands; and ⁴Chemical Engineering Department, School of Engineering, Aristotle University of Thessaloniki, Thessaloniki, Greece

Abstract

Boutsoukis C, Verhaagen B, Versluis M, Kastrinakis E, van der Sluis LWM. Irrigant flow in the root canal: experimental validation of an unsteady Computational Fluid Dynamics model using high-speed imaging. *International Endodontic Journal* 43, 393–403, 2010.

Aim To compare the results of a Computational Fluid Dynamics (CFD) simulation of the irrigant flow within a prepared root canal, during final irrigation with a syringe and a needle, with experimental high-speed visualizations and theoretical calculations of an identical geometry and to evaluate the effect of off-centre positioning of the needle inside the root canal.

Methodology A CFD model was created to simulate irrigant flow from a side-vented needle inside a prepared root canal. Calculations were carried out for four different positions of the needle inside a prepared root canal. An identical root canal model was made from poly-dimethyl-siloxane (PDMS). High-speed imaging of the flow seeded with particles and

Particle Image Velocimetry (PIV) were combined to obtain the velocity field inside the root canal experimentally. Computational, theoretical and experimental results were compared to assess the validity of the computational model.

Results Comparison between CFD computations and experiments revealed good agreement in the velocity magnitude and vortex location and size. Small lateral displacements of the needle inside the canal had a limited effect on the flow field.

Conclusions High-speed imaging experiments together with PIV of the flow inside a simulated root canal showed a good agreement with the CFD model, even though the flow was unsteady. Therefore, the CFD model is able to predict reliably the flow in similar domains.

Keywords: Computational Fluid Dynamics, high-speed imaging, irrigation, needle, Particle Image Velocimetry.

Received 23 September 2009; accepted 9 December 2009

Introduction

Irrigation of root canals with antibacterial solutions is considered an essential part of chemo-mechanical preparation (Haapasalo *et al.* 2005). Irrigation with a syringe and needle remains the most commonly used irrigation procedure (Ingle *et al.* 2002, Peters 2004). However, there is a general uncertainty about

the efficiency of this procedure in the narrow, most apical part of the root canal (Senia *et al.* 1971, Vande Visse & Brilliant 1975, Ram 1977). It has been argued that the limiting factor of the irrigation procedure is the difficulty to flush the apical root canal with large volumes of fresh irrigant (Druttman & Stock 1989).

To study this problem, attempts to evaluate the irrigant flow within the root canal have been attempted, based on macroscopic observations (Kahn *et al.* 1995, Peters & Peters 2005, Zehnder 2006). However, these studies of the fluid dynamics were limited because

Correspondence: Christos Boutsoukis, 29, Kimis Str., Kalamaria, 551 33 Thessaloniki, Greece (Tel.: +302310427813; fax: +302310999639; e-mail: chb@dent.auth.gr).

such a macroscopic approach can provide only a general description of the irrigant flow.

Computational fluid dynamics (CFD) represents a powerful tool to investigate flow patterns and physical and chemical phenomena by mathematical modelling and computer simulation (Tilton 1999, Arvand *et al.* 2005). Despite the fact that CFD was originally developed for industrial and engineering purposes, applications in the biomedical field have also attracted considerable attention (Yoganathan *et al.* 2005), aided by the increasing power of computers (Steinman 2002). CFD simulations can provide details on the velocity field in areas where experimental measurements are difficult to perform. Furthermore, important properties such as shear stress and pressure can easily be obtained, in contrast to experiments, especially in microscale flow problems. Recently, a CFD model was implemented for the evaluation of irrigant flow in the root canal (Boutsoukis *et al.* 2009). However, this model has not been validated yet through comparison to experimental data, a procedure that is considered essential for any model (Oberkampf & Trucano 2002). A similar model has also been introduced (Gao *et al.* 2009), but its validation lacked detail on the actual fluid dynamics.

Particle image velocimetry (PIV) is a well-established non-intrusive technique for the measurement of a velocity field. The displacement of small tracer particles added to a fluid is recorded by high-speed imaging and analysed using statistical correlation methods to extract the velocity distribution in the examined plane (Raffel *et al.* 2007). MicroPIV is a modification of PIV to access the small scales of microfluidic devices. High-speed imaging experiments have been performed in the

past to visualize and analyse the action of endodontic irrigation systems inside simulated root canals (De Groot *et al.* 2009, Jiang *et al.* 2009). However, this method has not been applied yet to the study of syringe irrigation in root canals.

The aim of this study was twofold: (i) to compare the results of a CFD simulation of the irrigant flow within a prepared root canal, during final irrigation with a syringe and needle, to high-speed visualizations, theoretical calculations and the results of a previous study (Boutsoukis *et al.* 2007a); (ii) to evaluate the effect of off-centre positioning of the needle inside the root canal, as it is likely to occur during the experimental part of this study and also under clinical conditions.

Materials and methods

CFD setup

The root canal was simulated as a geometrical frustum of a cone (the portion of a cone which lies between two parallel planes cutting the solid). The apical constriction and apical foramen were not simulated because they were not within the focus of this study. The apical terminus of the root canal was simulated as an impermeable wall. The length of the root canal model was 18 mm, the diameter was 1.57 mm at the canal orifice and 0.45 mm (ISO size 45) at the most apical point (6.2% taper) (Fig. 1). This shape is consistent with the root canal model used in the experimental setup.

The needle was modelled using the 30G KerrHawe Irrigation Probe (KerrHawe SA, Bioggio, Switzerland) as a reference, similarly to a previous study (Boutsoukis

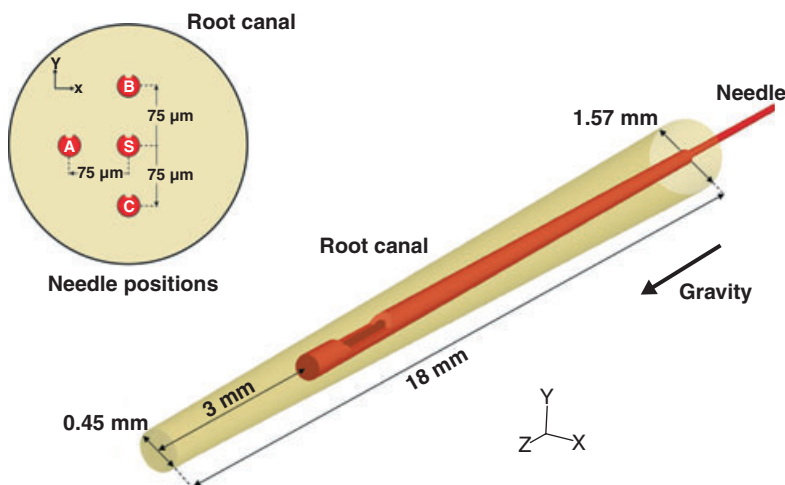


Figure 1 Geometrical characteristics of the computational fluid dynamics root canal model used. Off-center positions studied are depicted in the upper left circle.

et al. 2009). The external and internal diameter and the length were defined as $D_{\text{ext}} = 320 \mu\text{m}$, $D_{\text{int}} = 196 \mu\text{m}$, $l = 31 \text{ mm}$, respectively. The needle was fixed and centred within the canal, 3 mm short of the working length (Fig. 1 – case S). This setup allows for the evaluation of irrigant flow apically to the needle tip, the most challenging area for irrigation. Three additional cases were modelled to study the effect of off-centre positioning of the needle with respect to the longitudinal axis of the root canal. The needle was assumed to be displaced $75 \mu\text{m}$ away from the longitudinal axis towards the negative x , positive y or negative y direction (Fig. 1 – cases A, B and C respectively). In all cases, the needle remained parallel to the longitudinal axis of the root canal.

The pre-processor software Gambit 2.4 (Fluent Inc., Lebanon, NH, USA) was used to build the 3-D geometry and the mesh. No symmetry assumption was made for the flow domain. A hexahedral mesh was constructed and refined near the walls and in the areas where high gradients of velocity were anticipated, such as near the needle outlet. A grid-independency check was performed to determine the minimum number of computational cells required for a grid-independent flow simulation and ensure reasonable use of computational resources. The final mesh consisted of 587 417 cells (mean cell volume $2.6487 \times 10^{-5} \text{ mm}^3$). A similar mesh was used for all cases studied.

No-slip boundary conditions were applied to the walls of the root canal and that of the needle, under the hypothesis of rigid, smooth and impermeable walls. The fluid flowed into the simulated domain through the needle inlet and out of the domain through the root canal orifice, where atmospheric pressure was imposed. The canal and the needle were assumed to be completely filled with irrigant. A velocity inlet boundary condition was selected for the inlet of the needle. A flat velocity profile with a constant axial velocity of 8.6 m s^{-1} was imposed at the inlet, which is consistent with a clinically realistic irrigant flow rate of 0.26 mL s^{-1} through a 30G needle (Boutsioukis et al. 2007a). The irrigant was distilled water, and it was modelled as an incompressible Newtonian fluid with a density $\rho = 0.998 \text{ g cm}^{-3}$ and a viscosity $\mu = 1.0 \times 10^{-3} \text{ Pa s}$ (Lide 2005). Gravity was included in the flow field in the direction of the positive z axis.

The commercial CFD code FLUENT 6.3 (Fluent Inc.) was used to set up and solve the problem and to analyse the results. The uncoupled Navier–Stokes equations which describe the time-dependent, three-dimensional, incompressible flow were solved by an

implicit iterative solver. The numerical solution method uses a finite volume approach. An unsteady isothermal flow was assumed; steady-state solutions were obtained first, then used as initial conditions for the unsteady simulations, to avoid transient effects. No turbulence model was used, as the flow under these conditions (Reynolds number $Re = 1678$ inside the needle lumen) was expected to be laminar (Boutsioukis et al. 2009). All transport equations were discretized to be at least second-order accurate. A time-step of 10^{-6} s was used throughout the calculations, which were carried out for a real flow time of 50 ms for each of the four cases. The convergence criterion of the maximum scaled residuals was set at 10^{-4} . Pressure, velocity and vorticity in selected areas of the flow domain were also monitored to ensure adequate convergence in every time-step. Computations were carried out in a computer cluster (45 dual core AMD Opteron 270 processors) running 64-bit SUSE Linux 10.1 (kernel version 2.6.16).

The instantaneous and time-averaged velocity field for selected time-points (case S) were extracted and compared to results obtained in the experimental section of this study. The time-averaged velocity field for cases A, B and C was also extracted and compared to each other and to case S. An additional assessment of the validity of the CFD model was attempted through comparison of the theoretical velocity profile inside the needle lumen (Kundu & Cohen 2004) to the CFD results, 1 mm coronally to the needle outlet, assuming a fully developed laminar flow at that point. The time-averaged pressure at the needle inlet was also extracted and compared to the results of a previous study (Boutsioukis et al. 2007a).

Experimental setup

A transparent root canal model was fabricated using poly-dimethyl-siloxane (PDMS) (Sylgard[®] 184, Silicone Elastomer kit; Dow Corning, Coventry, UK). The polymer was mixed at a base:curing agent ratio of 15 : 1. To obtain specific dimensions of the root canal, a modified D-size finger spreader (Dentsply Maillefer, Ballaigues, Switzerland) was used. This instrument has a tip diameter of 0.31 and a 6.2% taper, determined under stereoscopic microscope. A 2.2-mm section from the tip of the spreader was carefully removed to increase the tip diameter to 0.45 mm. The PDMS root canal had a total length of 18 mm. These dimensions match the root canal as simulated in the CFD model.

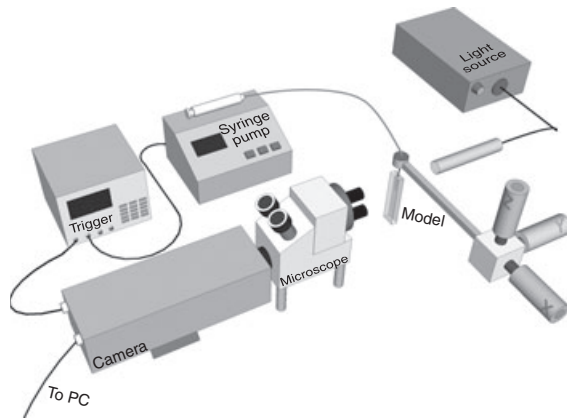


Figure 2 Schematic diagram of the experimental high-speed visualization setup.

For the high-speed imaging, a high-speed camera (Shimadzu HPV-1; Shimadzu Corp., Kyoto, Japan), capable of recording up to 10^6 frames s^{-1} , was attached to an optical microscope (BX-FM; Olympus Corp., Tokyo, Japan) (Fig. 2). Immediately before use, the model was rinsed thoroughly with 95% ethanol and left to dry, and then fitted in front of the microscope.

A side-vented endodontic needle (30G KerrHawe Irrigation Probe, KerrHawe SA, Bioggio, Switzerland) was attached to a Luer-Lock T-connector, which was mounted on a micrometric translation stage (9067M; New Focus, San Jose, CA, USA and M-044.00; Physik Instrumente, Karlsruhe, Germany) capable of adjusting its position in three directions and tilting around two axes. This setup ensured accurate and stable positioning of the needle inside the model. In addition, a rubber stop was applied to indicate the desired depth of penetration of the needle. The needle was placed 3 mm from the apical terminus of the canal and at the best centre position possible.

Two different views of the needle were studied: side view, with the needle outlet at right angle to the lens, and front view, with the outlet oriented towards the objective lens. An $1.25\times$ objective lens (PlanApoN $1.25\times$; Olympus Corp.) was used to assist positioning of the needle with accuracy, while a $10\times$ objective lens (MPlanN $10\times$; Olympus Corp.) was used for image recording. The microscope was focused at the centre plane of the canal, guided by the major perimeter of the needle. The depth of focus of the objective was calculated to be approximately $120\ \mu\text{m}$ (Meinhart *et al.* 2000) which indicates that the particle movement captured was limited to a shallow plane with thickness of approximately one-fifth of the root canal diameter

and 10 times the particle diameter. This depth was considered a sufficient experimental approximation to the infinitely shallow plane used by the CFD software to report velocity distribution. Light was provided for bright-field imaging by a high-intensity continuous cold-light source (ILP-1; Olympus Corp.).

The T-connector was further connected through a thick-walled Teflon tubing to a 20-mL disposable syringe with a Luer-Lock connector (Plastipak; Becton Dickinson, Oxford, UK). A programmable precision syringe pump (NE-1010; New Era Pump Systems, Wantagh, NY, USA) was used to deliver irrigant at the precise rate of $0.26\ \text{mL}\ s^{-1}$, to maintain irrigation consistency. Distilled water at room temperature was used as an irrigant. Hollow-glass spherical particles (mean diameter $11\ \mu\text{m}$, mean density $1.1 \times 10^3\ \text{kg}\ \text{m}^{-3}$) (Spherichel[®]; Potters Industries, Barnsley, UK) were added to the irrigant at a concentration of $10\ \text{mg}\ \text{mL}^{-1}$ to allow visualization of the flow inside the simulated root canal. The syringe was filled prior to each experiment with special care taken to avoid insertion of air into the system. The fluid was stirred continuously by a custom-made magnetic stirrer to avoid precipitation of particles. Between successive recordings, the needle, connecting tube, T-connector and model were flushed with distilled water to prevent particle accumulation.

The camera was triggered 4 s after the start of the syringe pump, using a pulse and delay generator (BNC-565; Berkeley Nucleonics, San Rafael, CA, USA). Images were recorded at a speed up to 250 000 frames s^{-1} at three different parts of the experimental root canal model for both the front view and the side view (Figs 3 and 4, positions I–III). The exposure time was set to one-eighth of the interframe time, which corresponded to 500 ns for the highest frame rate. Recordings were transferred to MATLAB (The Mathworks, Natick, MA, USA) and were analysed using in-house built PIV code. Several frames from a single recording were ensemble-averaged before being analysed. The resulting velocity fields in the two orthogonal planes (side view and front view) were compared to the CFD results regarding velocity direction and magnitude.

Results

Validation of the CFD model

The flow field within the canal revealed an unsteady behaviour, as determined by both the CFD simulation (Fig. 5, Movie S1) and the PIV experiments. The normalized standard deviation of the time-averaged

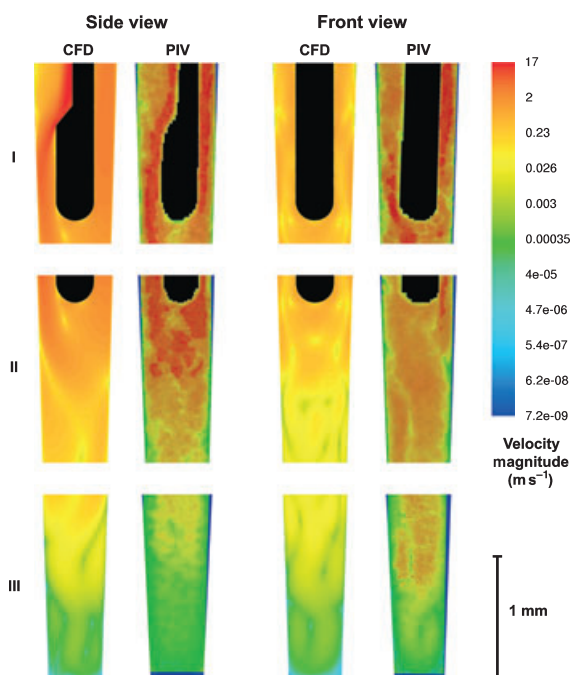


Figure 3 Contours of velocity magnitude along the z - y (side-view) and z - x (front view) plane of the domain for case S. Lower velocity regions, like the center of vortices, show up as lighter areas. A good agreement between computational fluid dynamics and particle image velocimetry (PIV) results is evident in most of the domain studied. PIV results close to the wall of the root canal (dark blue stripes) are not considered accurate due to inherent limitations of the PIV method. The needle wall is coloured black.

velocity magnitude, which is a measure of the unsteadiness of the flow, was calculated in the range 0.001–10 times the local time-averaged velocity, with very few points reaching a value of 500.

Comparison of the velocity magnitude and vectors (Figs 3 and 4) in the z - y plane (side view) and z - x plane (front view) between CFD calculations and experiments revealed a close agreement in terms of velocity magnitude and vortex location and size. The direction of the vortices near the boundary of adjacent positions was also in good agreement (Fig. 4I–III), even though the results for each positions were based on separate recordings. The main characteristic bands occurred in regions where the velocity was high. The vector images resulting from both the CFD and the experiments (Fig. 4) showed a number of Moffatt vortices (Moffatt 1964), which were driven by the flow from the needle outlet around the tip.

To test the inflow conditions, the theoretical and the CFD velocity profile inside the needle lumen were

compared (Fig. 6). The two profiles were almost identical with differences smaller than 1%.

The time-averaged pressure at the inlet of the needle for the period $t = 0$ –50 ms as calculated by the CFD model was 244.0 ± 0.5 kPa. The average intrabarrel pressure recorded close to the needle inlet for the same irrigant flow rate during a previous study (Boutsioukis et al. 2007a) was 232.2 ± 23.6 kPa.

Effect of off-centre positioning of the needle

Comparison of the velocity magnitude in the z - y plane (side view) and z - x plane (front view) as calculated by the CFD model for cases A, B and C showed that small displacements from the central position may have a limited effect on the flow field (Fig. 7). Some differences in magnitude were found near the apical terminus of the canal, where the increase in velocities was up to two orders of magnitude compared to case S.

Comparison of the velocity vectors in the z - y plane (side view) and z - x plane (front view) for different needle positions (Fig. 8) revealed that the flow pattern in the z - y plane was not greatly affected by off-centre positioning of the needle. Most of the vortices formed in case S also appeared in cases A, B and C in almost identical positions. In the z - x plane, the symmetry that was observed close to the needle tip in cases S, B and C was absent in case A. This resulted in a flow pattern similar to the one observed during the experiments, where the needle was slightly displaced from the centre of the canal (Fig. 4, Front view, PIV, I).

Discussion

In this study, irrigant flow inside a root canal was evaluated by a previously published CFD model that was modified, and a microPIV setup. Comparison of the detailed flow field resulting from CFD and PIV was performed to assess the validity of the CFD model.

A simple root canal geometry resembling the prepared root canal of a maxillary central incisor was used, to facilitate manufacturing of an accurate PDMS model for the experiments. The geometrical complexity of a CFD model is only limited by the intentions of the researcher and the computational resources available, in contrast to the manufacturing of root canals in resin blocks or PDMS. Clinically realistic CFD models of arteries and respiratory tracts have already been constructed using MRI scans (Steinman 2002, Xu et al. 2006, Wang et al. 2007). An additional advantage of CFD modelling is the ability to create strictly

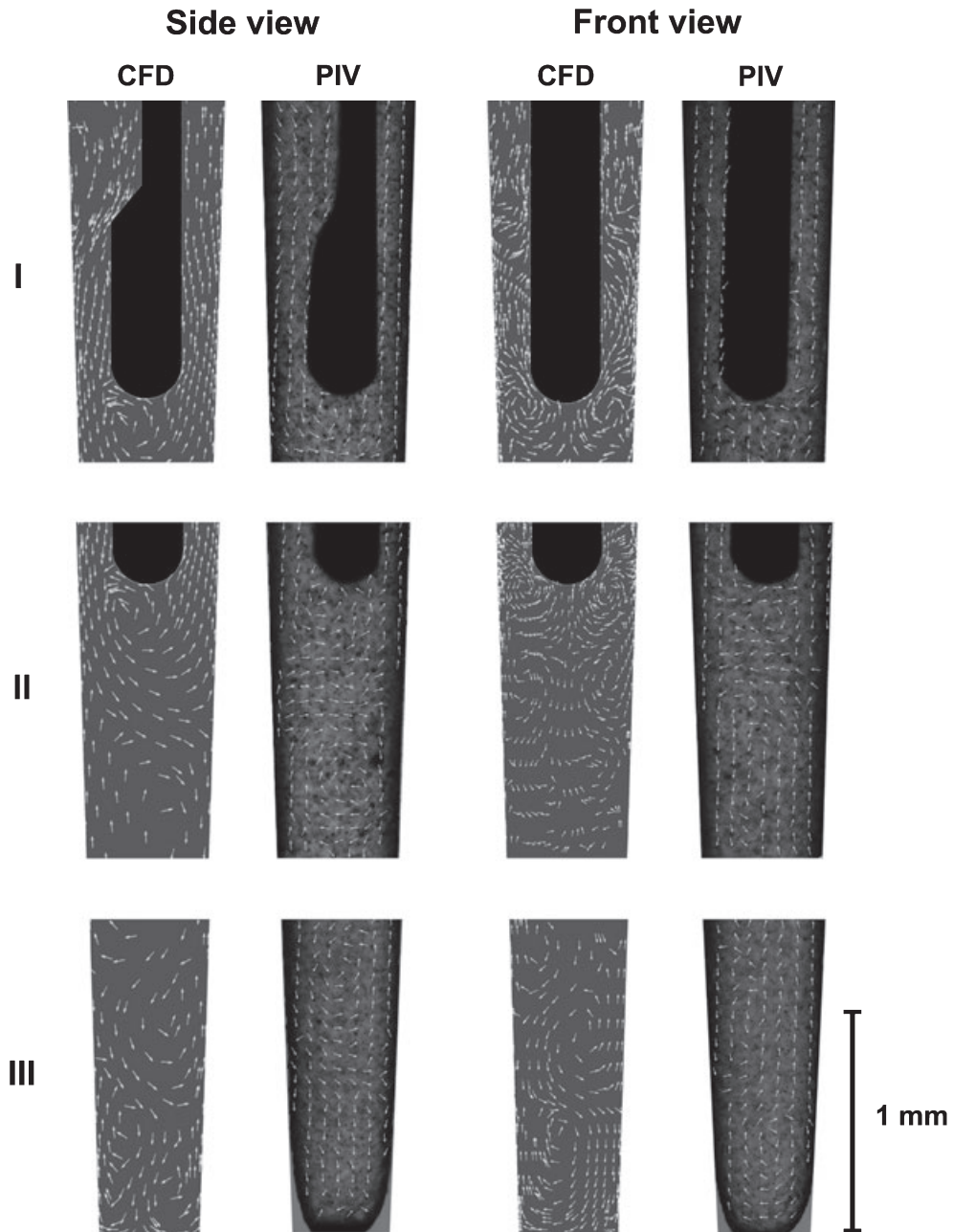


Figure 4 Velocity vectors along the z - y (side-view) and z - x (front view) plane of the domain for case S. Only the direction and not the magnitude of the velocity is depicted. A good agreement between computational fluid dynamics and particle image velocimetry (PIV) results regarding the direction of velocity is shown. The needle wall is coloured black.

standardized root canals regardless of the desired complexity, and evaluate the isolated effect of different parameters on the flow. However, only one parameter should be modified and evaluated in each set of CFD simulations and the overall complexity of the model should be gradually increased during this procedure. In

this way, a clear correlation between each change in the geometry and the resulting change in the flow can be established.

In the current CFD model, no assumption was made about the symmetry of the flow inside the root canal, in contrast to an earlier study (Boutsioukis *et al.* 2009). It

Figure 5 Overview of the results of the CFD calculations for case S. (a–c) Contours of instantaneous velocity magnitude at $t = 10, 30$ and 50 ms respectively. (d) Time-averaged velocity magnitude (e). Standard deviation of the time-averaged velocity magnitude normalized with the time-averaged velocity magnitude (f). Time-averaged velocity vectors. The needle wall is coloured black. (Case S, z - y plane).

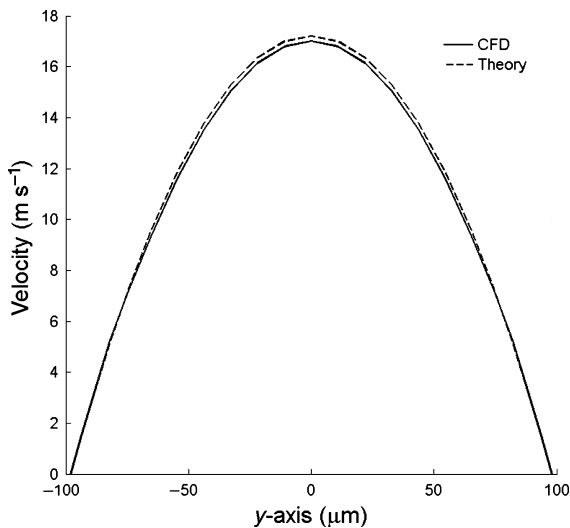
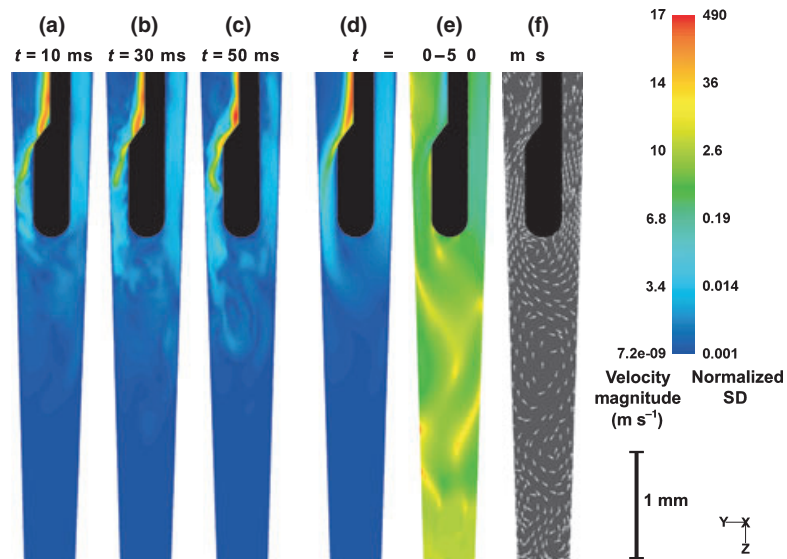


Figure 6 Comparison of the theoretical velocity profile inside the needle lumen to the CFD results, 1 mm coronally to the needle outlet, assuming a fully-developed laminar flow at that point. The two profiles are almost identical with differences smaller than 1%.

can be speculated that this assumption is valid for low velocities, but there is an increasing possibility of symmetry-breaking downstream of a sudden expansion of the flow domain – such as the area of the root canal near the needle outlet – as the velocity of the fluid increases, even for a steady flow rate (Sherwin & Blackburn 2005, Mullin *et al.* 2009). This modification is considered to increase the accuracy and validity of the model.

In addition, the flow was simulated in an unsteady, time-dependent manner, which more closely resembles real conditions. In both the computational and experimental elements of this study it was confirmed that the flow of the irrigant under the conditions described is unsteady (Fig. 5, Movie S1). The flow parameters were averaged over a time period of 50 ms to distinguish the most stable characteristics of the flow, which are relevant for replacement of irrigant, thereby probably omitting transient flow characteristics. This modification is also considered to increase the accuracy and validity of the model. Nevertheless, significantly more computational resources were required to make these modifications possible, which were not available during the previous study (Boutsioukis *et al.* 2009). Comparison of the previous study with the time-averaged velocities from the current unsteady simulation revealed small differences.

The internal diameter of the needle used has been reported to be 168 μm (Boutsioukis *et al.* 2007b). However, the presence of irregularities on the internal surface has also been reported to hinder accurate measurements of the internal diameter and increase the uncertainty (Boutsioukis *et al.* 2007b). In this study, the methodology described by Boutsioukis *et al.* (2007b) was combined with measurement of the pressure drop across the needle for known flow rates (data not shown), according to the methodology of another study (Boutsioukis *et al.* 2007a), to determine the internal needle diameter as accurately as possible. Results of these preliminary experiments showed that the internal diameter should be adjusted to 196 μm in

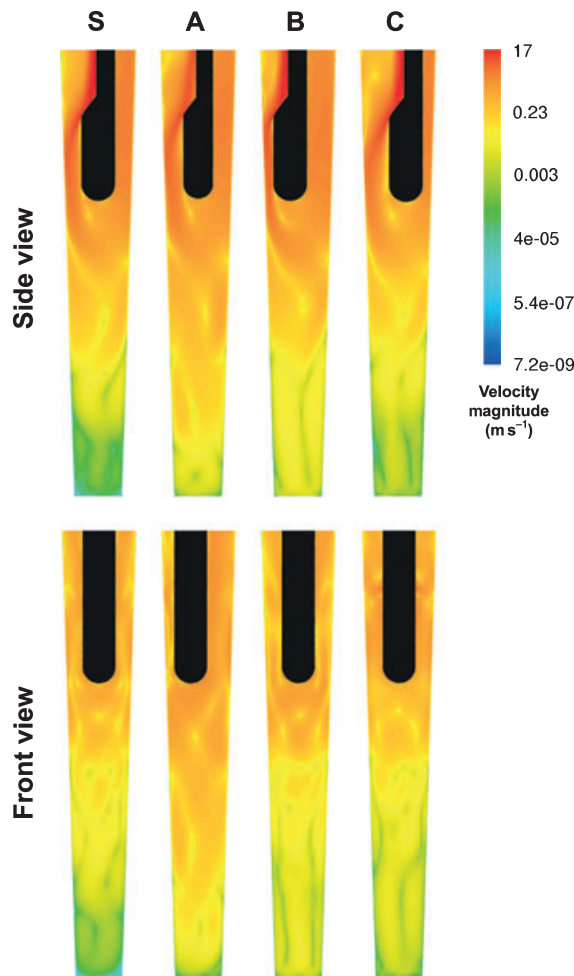


Figure 7 Time-averaged velocity magnitude along the z - y (side-view) and z - x (front view) plane of the domain for cases S, A, B and C, according to CFD calculations. Small displacements from the central position had a limited effect on the velocity magnitude. The needle wall is coloured black.

the CFD model. Close agreement of the CFD results on pressure drop along the needle with a previous experimental study (Boutsoukis *et al.* 2007a) and with the preliminary experiments conducted revealed that the determined internal diameter was correct.

The release of neutrally buoyant tracer particles within the flow is a procedure that aids enhanced visualization of the flow pattern. Such particles are expected to follow the path of the fluid with accuracy (Tilton 1999, Raffel *et al.* 2007). A conventional PIV setup makes use of a laser sheet to illuminate fluorescent tracer particles to visualize and analyse the flow. In the present microPIV setup, an objective with a

small depth of focus and a continuous light source were used instead of a laser sheet. The main advantage of this setup was that the recording speed was not restricted by the amount of light emitted from fluorescent particles. Therefore, recordings could be made both at high recording speeds and for a prolonged time (100 frames). A prolonged recording time allowed for ensemble averaging, which reduces the noise in the individual PIV recordings (Raffel *et al.* 2007).

Nevertheless, according to the CFD results, velocities up to 17 m s^{-1} appeared near the needle outlet but such high velocities were rarely identified in the PIV results. It is possible that only a few particles acquired such high velocities and because of ensemble averaging performed by the PIV code, calculated velocities appeared lower. Manual tracking of individual particles revealed that velocities at least up to 13 m s^{-1} were indeed present in the experiments. Moreover, measured velocities close to the wall appeared to be lower than the computed velocities. This can be attributed to an inherent limitation of PIV, which uses an interrogation area to calculate the velocity, instead of a single point (Raffel *et al.* 2007). In the immediate vicinity of the wall, the interrogation area is partly comprised of the flow domain and partly of the wall. Therefore, averaging over this area is expected to reduce the average velocity (Usera *et al.* 2004).

The assumption of smooth walls of both the root canal and the needle in the CFD model is inconsistent with real dentine anatomy and to the findings of a previous study (Boutsoukis *et al.* 2007b). Wall roughness is expected to have a limited effect on pressure drop as long as the flow remains laminar (McCabe *et al.* 2004), but it may induce vorticity or even turbulence in the flow (Azuma & Hoshino 1985). Scanning electron microscopy examination of the PDMS model used in the experiments revealed that its surface presented irregularities $3\text{--}6 \mu\text{m}$ wide (data not shown), which were in the order of magnitude of the dentinal tubule orifices. However, no turbulence was noticed during the experiments with these models. Furthermore, the surface of PDMS is naturally hydrophobic (Bodas & Khan-Malek 2006). Yet, PDMS is the most widely used material in the construction of microfluidic devices. During a pilot study, oxygen plasma was used to modify the surface of PDMS models and increase its hydrophilicity, as suggested in the literature (Bodas & Khan-Malek 2006). However, no measureable difference was noted in the flow as a result of this treatment and it was therefore excluded from the main experimental protocol.

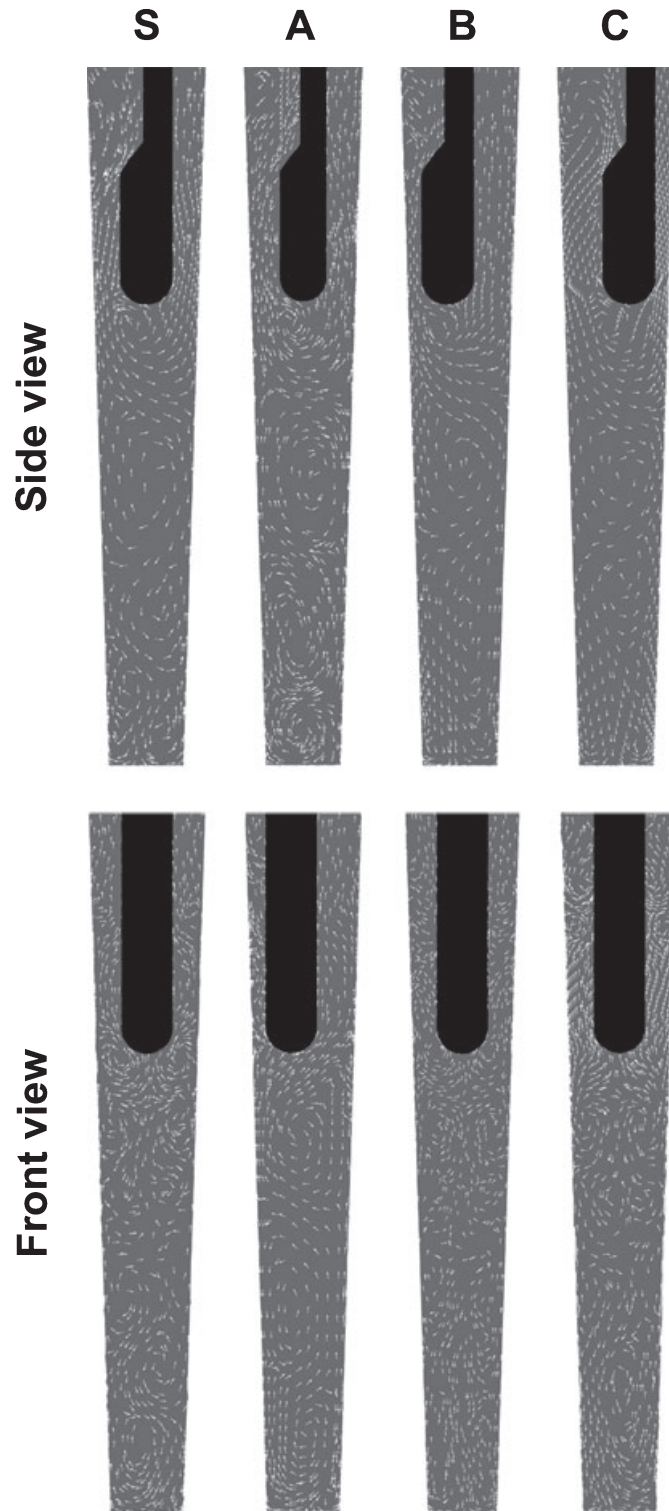


Figure 8 Velocity vectors along the z - y (side-view) and z - x (front view) plane of the domain for cases S, A, B and C, according to CFD calculations. Only the direction and not the magnitude of the velocity is depicted. The flow pattern in the z - y plane is not affected by off-center positioning of the needle. The symmetry observed in the z - x plane close to the needle tip in cases S, B and C is absent in case A. The needle wall is coloured black.

Both in the CFD model and in the experiments, distilled water was used as irrigant. NaOCl solutions used during routine endodontic treatment have physical properties very similar to those of water (Guerisoli et al. 1998, Lide 2005), and should therefore exhibit the same flow characteristics. Furthermore, significant experimental disadvantages, such as oxidation of metal parts and crystal precipitation were noted during a previous study during which NaOCl was used (Boutsioukis et al. 2007a). In addition, NaOCl might affect the surface of the PDMS model.

In spite of the precise alignment of the needle inside the PDMS model, the possibility of small displacements from the central position could not be excluded. Such displacements are also expected during a clinical irrigation procedure. Therefore, the effect of such small displacements on the flow inside the root canal model was studied by the additional CFD cases (A, B and C). Off-centre positioning may affect the overall flow pattern. Positioning the needle closer to canal wall generally resulted in slightly increased velocities apically to the needle tip, most noticeably near the apical terminus of the canal (Fig. 7). The more limited space available laterally to the needle in these cases possibly resulted in this increase in velocities. However, it is doubtful whether these differences can have a significant effect on clinically relevant parameters such as irrigant replacement, shear stress on the canal wall and irrigant pressure at the apical foramen.

The agreement between CFD and PIV results regarding velocity vectors in the front view was not exact (Fig. 4). This could be attributable to small displacements of the needle from the central position during experiments. Moreover, the highest velocities and most consistent flow pattern occurred in the z - y plane, which makes the experimental results in the z - x plane more dependent on the focal position of the microscope.

A detailed description of the flow and its relevance to root canal debridement and disinfection was not included in this study, as the aim was to assess the validity of the CFD model. A validated CFD model can be used to predict the flow not only in the domain used for validation but also in similar and more complicated flow domains, which is an additional advantage over experimental methods. The absence of turbulence that was verified in both CFD and experimental sections of this study (Reynolds number in the order of 1500) provides further confidence about the validity of the CFD model in such flow domains. This CFD model will be used in subsequent studies to evaluate the effect of

various factors on the fluid dynamics during root canal irrigation.

Conclusions

High-speed imaging experiments together with PIV analysis of the flow inside a simulated root canal have shown a good agreement with the velocity field as calculated by a CFD model, even though the flow was unsteady. Therefore, the CFD model is able to predict reliably the flow in similar domains. Small lateral displacements of the needle inside the canal had a limited effect on the flow.

Acknowledgements

The authors are grateful to B. Benschop, T. Tsilipiras and A. Werner for valuable technical assistance, and to D. van der Meer and N.G. Deen, for valuable discussions. This study was partially funded through a Scholarship for Excellent PhD Students from the Research Committee of Aristotle University of Thessaloniki, Greece (C.B.) and through Project 07498 of the Dutch Technology Foundation STW (B.V.).

References

- Arvand A, Hormes M, Reul H (2005) A validated computational fluid dynamics model to estimate hemolysis in a rotary blood pump. *Artificial Organs* **29**, 531–40.
- Azuma T, Hoshino T (1985) The radial flow of a thin liquid film (5th report, influence of wall roughness on laminar-turbulent transition). *Bulletin of Japan Society of Mechanical Engineers* **28**, 1682–9.
- Bodas D, Khan-Malek C (2006) Formation of more stable hydrophilic surfaces of PDMS by plasma and chemical treatments. *Microelectronic Engineering* **83**, 1277–9.
- Boutsioukis C, Lambrianidis T, Kastrinakis E, Bekiaroglou P (2007a) Measurement of pressure and flow rates during irrigation of a root canal ex vivo with three endodontic needles. *International Endodontic Journal* **40**, 504–13.
- Boutsioukis C, Lambrianidis T, Vasiliadis L (2007b) Clinical relevance of standardization of endodontic irrigation needle dimensions according to the ISO 9626:1991 & 9626:1991/ Amd 1:2001 specification. *International Endodontic Journal* **40**, 700–6.
- Boutsioukis C, Lambrianidis T, Kastrinakis E (2009) Irrigant flow within a prepared root canal using different flow rates: a Computational Fluid Dynamics study. *International Endodontic Journal* **42**, 144–55.
- De Groot SD, Verhaagen B, Versluis M, Wu M-K, Wesseling PR, van der Sluis LWM (2009) Laser-activated irrigation of

- the root canal: cleaning efficacy and flow visualization. *International Endodontic Journal* **42**, 1077–83.
- Druttman ACS, Stock CJR (1989) An in vitro comparison of ultrasonic and conventional methods of irrigant replacement. *International Endodontic Journal* **22**, 174–8.
- Gao Y, Haapasalo M, Shen Y *et al.* (2009) Development and validation of a three-dimensional Computational Fluid Dynamics model of root canal irrigation. *Journal of Endodontics* **35**, 1282–7.
- Guerisoli DMZ, Silva RS, Pecora JD (1998) Evaluation of some physico-chemical properties of different concentrations of sodium hypochlorite solutions. *Brazilian Endodontic Journal* **3**, 21–3.
- Haapasalo M, Endal U, Zandi H, Coil JM (2005) Eradication of endodontic infection by instrumentation and irrigation solutions. *Endodontic Topics* **10**, 77–102.
- Ingle JI, Himel VT, Hawrish CE *et al.* (2002) Endodontic cavity preparation. In: Ingle JI, Bakland LK, ed. *Endodontics*, 5th edn. Ontario, Canada: BC Decker, pp. 502.
- Jiang L-M, Verhaagen B, Versluis M, van der Sluis LWM (2010) Evaluation of a sonic device designed to activate irrigant in the root canal. *Journal of Endodontics* **36**, 143–6.
- Kahn FH, Rosenberg PA, Gliksberg J (1995) An in vitro evaluation of the irrigating characteristics of ultrasonic and subsonic handpieces and irrigating needles and probes. *Journal of Endodontics* **21**, 277–80.
- Kundu PK, Cohen IM (2004) *Fluid Mechanics*, 3rd edn. San Diego, CA, USA: Elsevier Academic Press, pp. 283–5.
- Lide DR (2005) *CRC Handbook of Chemistry and Physics*, 86th edn. Boca Raton, FL, USA: CRC Press, 6.2 pp.
- McCabe WL, Smith JC, Harriott P (2004) *Unit Operations of Chemical Engineering*, 7th edn. New York, USA: McGraw-Hill, pp. 45–67, 98–132, 244–98, 929–65.
- Meinhart CD, Wereley ST, Gray MHB (2000) Volume illumination for two-dimensional particle image velocimetry. *Measurement Science and Technology* **11**, 809–14.
- Moffatt HK (1964) Viscous and resistive vortices near a sharp corner. *Journal of Fluid Mechanics* **18**, 1–18.
- Mullin T, Seddon JRT, Mantle MD, Sederman AJ (2009) Bifurcation phenomena in the flow through a sudden expansion in a circular pipe. *Physics of Fluids* **21**, 014110.
- Oberkampf WL, Trucano TG (2002) Verification and validation in computational fluid dynamics. *Progress in Aerospace Sciences* **38**, 209–72.
- Peters OA (2004) Current challenges and concepts in the preparation of root canal systems: a review. *Journal of Endodontics* **30**, 559–67.
- Peters OA, Peters CI (2005) Cleaning and shaping of the root canal system. In: Cohen S, Hargreaves KM, eds. *Pathways of the Pulp*, 9th edn. St. Louis, USA: Mosby, 325 pp.
- Raffel M, Willert C, Wereley S, Kompenhans J (2007) *Particle Imaging Velocimetry – A Practical Guide*, 2nd edn. Berlin, Germany: Springer, pp. 1–448.
- Ram Z (1977) Effectiveness of root canal irrigation. *Oral Surgery, Oral Medicine, Oral Pathology* **44**, 306–12.
- Senia ES, Marshall JF, Rosen S (1971) The solvent action of sodium hypochlorite on pulp tissue of extracted teeth. *Oral Surgery, Oral Medicine, Oral Pathology* **31**, 96–103.
- Sherwin SJ, Blackburn HM (2005) Three-dimensional instabilities and transition of steady and pulsatile axisymmetric stenotic flows. *Journal of Fluid Mechanics* **533**, 297–327.
- Steinman DA (2002) Image-based Computational Fluid Dynamics modeling in realistic arterial geometries. *Annals of Biomedical Engineering* **30**, 483–97.
- Tilton JN (1999) Fluid and particle dynamics. In: Perry RH, Green DW, Maloney JO, ed. *Perry's Chemical Engineer's Handbook*, 7th edn. New York, USA: McGraw-Hill, pp. 6.1–50.
- Usera G, Vernet A, Ferré JA (2004) Considerations and improvements of the analysing algorithms used for time resolved PIV of wall bounded flows. In: Proceedings of the 12th International Symposium on Applications of Laser Techniques to Fluid Mechanics, Lisbon, July 11–15. http://in3.dem.ist.utl.pt/lxaser2004/pdf/paper_24_3.pdf.
- Vande Visse JE, Brilliant JD (1975) Effect of irrigation on the production of extruded material at the root apex during instrumentation. *Journal of Endodontics* **1**, 243–6.
- Wang C, Pekkan K, De Zélicourt D *et al.* (2007) Progress in the CFD modeling of flow instabilities in anatomical total cavopulmonary connections. *Annals of Biomedical Engineering* **35**, 1840–56.
- Xu C, Sin SH, McDonough JM *et al.* (2006) Computational fluid dynamics modeling of the upper airway of children with obstructive sleep apnea syndrome in steady flow. *Journal of Biomechanics* **39**, 2043–54.
- Yoganathan P, Chandran KB, Sotiropoulos F (2005) Flow in prosthetic heart valves: state-of-the-art and future directions. *Annals of Biomedical Engineering* **33**, 1689–94.
- Zehnder M (2006) Root canal irrigants. *Journal of Endodontics* **32**, 389–98.

Supporting Information

Additional Supporting Information may be found in the online version of this article:

Movie S1. Contours of instantaneous velocity magnitude (m s^{-1}) along the z - y plane (side view) of the domain for case S ($t = 0$ –50 ms), according to CFD calculations. Unsteady behavior of the flow is evident. The needle wall is coloured white.

Please note: Wiley-Blackwell are not responsible for the content or functionality of any supporting materials supplied by the authors. Any queries (other than missing material) should be directed to the corresponding author for the article.